

Dark matter electromagnetic dipoles: the WIMP expectation

Thomas Hambye and Xun-Jie Xu

Service de Physique Théorique, Université Libre de Bruxelles, Boulevard du Triomphe, CP225, 1050 Brussels, Belgium

ABSTRACT: We perform a systematic study of the electric and magnetic dipole moments of dark matter (DM) that are induced at the one-loop level when DM experiences four-fermion interactions with Standard Model (SM) charged fermions. Related to their loop nature these moments can largely depend on the UV completion at the origin of the four-fermion operators. We illustrate this property by considering explicitly two simple ways to generate these operators, from t - or s -channel tree-level exchange. Fixing the strength of these interactions from the DM relic density constraint, we obtain in particular a magnetic moment that, depending on the interaction considered, lies typically between 10^{-20} to 10^{-23} ecm or identically vanishes. These non-vanishing values induce, via photon exchange, DM-nucleus scattering cross sections that could be probed by current or near future direct detection experiments.

Contents

1	Introduction	1
2	Framework	3
2.1	Effective interactions of DM	3
2.2	DM relic abundance	4
3	Loop-induced electromagnetic interactions	5
3.1	Closing the loop	5
3.2	A UV complete example	8
3.3	Expected magnitude of electromagnetic dipoles	10
4	Electromagnetic dipoles in direct detection	10
5	Conclusion	17
A	Loop calculations	17

1 Introduction

Weakly interacting massive particles (WIMPs) are among the best motivated dark matter (DM) candidates. As is well known, DM particles annihilating into lighter particles with coupling strength of order unity undergo a non-relativistic freeze-out in the primordial thermal bath of the Universe, leaving a relic density of the order of the observed one if the DM mass is roughly around the electroweak scale. This “WIMP miracle” has triggered vast experimental effort in DM searches—see [1–6] for reviews. In particular, over the past years, direct and indirect detection experiments have reached the sensitivity necessary to probe this paradigm in many different contexts. Collider experiments also offer possibilities of tests. A number of explicit models have been already excluded, whereas many other ones could be seriously tested in the near future.

In many models WIMPs annihilate into SM fermions via a t - or s -channel mediator. If this mediator is sufficiently heavy, it can be integrated out, leading to a local effective interaction. Thus in this case the (tree level) phenomenology of the model reduces to the one that can be obtained from the effective field theory (EFT) for DM annihilation. As is well-known too, in this case one can get a one-to-one relation between the annihilation rate fixed by the relic density constraint and direct, indirect as well as collider signals.¹

In this work we are interested in effective interactions involving charged SM fermions (f) and DM fermions (χ), of the general form $\mathcal{L} \supset G \bar{\chi} \mathcal{O} \chi \bar{f} \mathcal{O}' f$ with \mathcal{O} and \mathcal{O}' any possible

¹Actually, the criteria of having a sufficiently heavy mediator for the EFT to be valid depends on the process considered, see e.g. [7–9].

operators. From the relic density constraint the dimensional coupling G is typically of the order of $10^{-1}G_F \times (m_\chi/100 \text{ GeV})$ where G_F is the Fermi constant and m_χ is the DM mass. If the SM fermion is a light quark and DM lies around the electroweak scale, such values of G have already been ruled out by recent direct detection experiments for operators that lead to spin-independent (SI) cross sections on nuclei. These are in particular the XENON-1T [10], LUX [11] and PandaX-II [12] experiments which have now put upper limits on the SI DM-nucleon cross section down to $\sim 10^{-46} \text{ cm}^2$ for m_χ ranging from tens to hundreds of GeV. However, WIMPs are not necessarily expected to dominantly couple to light quarks. For other SM fermions (e.g. $f = e, \mu, \tau, c, b, t, \nu_e, \nu_\mu, \nu_\tau$), direct detection bounds are generally weaker. In addition, various operators may lead to spin-dependent (SD) cross sections, for which the experimental sensitivity is weaker.

An interesting possibility to improve the direct detection sensitivity in such cases stems from the fact that WIMPs might have electromagnetic dipole moments. In fact, various electromagnetic form factors (electric/magnetic dipoles, anapole, charged radius) of WIMPs have been considered in the literature [13–32]. Early studies [17–20, 24] considered them as a solution to resolve the discrepancy between DAMA/CoGeNT signals and null results of other DM searches, though this has been since then well excluded. Collider, γ -ray, and CMB searches for dipole interacting DM have been studied in Ref. [20, 21]. More recently, Ref. [28] considered leptophilic DM and showed that its loop-induced electromagnetic dipoles led to restrictive direct detection bounds.²

In this work, instead of considering that the annihilation induced by the dipole (into SM charged particles via photon exchange) is responsible for the relic density, as in many of these works (e.g. [15, 17–20]), or instead of assuming a specific model, we will instead start, as in Ref. [16], from the effective four-fermion operators. Once the coefficients of the effective operators are fixed by the relic density, we can compute the dipoles they lead to at the one-loop level (simply from closing the charged fermion line, and attaching an external photon). Actually, since dipoles are loop-level effects, the use of an effective theory to compute them is not necessarily consistent with what we would obtain in UV complete models. If the effective theory holds for arbitrarily high energy scales, the loop integral that leads to the dipoles would be divergent and such divergences cannot be canceled (absorbed) by any counterterms. Unlike for the annihilation process, one thus needs to open the effective interactions. We consider two straightforward ways to generate these effective interactions at tree level, namely s - or t -channel exchange. This leads to two general classes of models depending on whether they give a vanishing (as in the s -channel case) or a non-vanishing finite (as in the t -channel case) result. We argue that the results obtained for non-vanishing dipoles are generic, which is illustrated by comparing these results with the ones obtained in a UV complete model.

We then study the implication of non-vanishing dipole for direct detection. We find that the magnitude of the non-vanishing loop-induced dipoles, typically of the order of 10^{-20} ecm (or $10^{-20} m_f/m_\chi \text{ ecm}$), implies that DM-nucleus scattering via dipole interactions could be

²Beyond the WIMP regime, there has been growing interest in electromagnetic dipoles of sub-GeV DM due to potential connections with CMB/LSS observations, stellar physics, and the intensity frontier searches—see, e.g., [29–32].

probed within current and future experimental sensitivities. In particular for operators involving heavy quarks or charged leptons, or when the DM-nucleus cross section is SD at tree level, this might provide the best possibility of probing these interactions and thus possibly the origin of the DM relic density. This stems from the fact that for low nuclear recoil energies the cross section is considerably enhanced by the exchange of a massless (photon) mediator.

The paper is organized as follows. In Sec. 2, we present a complete description of the most general four-fermion interactions of DM fermions with SM fermions, and determine the interaction strength required to produce the observed relic abundance. Given the determined interaction strength, in Sec. 3, we compute the loop-induced electromagnetic dipoles of DM by closing charged fermion loops in the four-fermion interactions, assuming that they are induced by either t -channel or s -channel tree level exchange. There we also compare the results obtained in this way to the ones obtained from considering an explicit UV complete model. In Sec. 4, the resulting magnitude of electromagnetic dipoles is confronted with direct detection limits obtained by investigating the recoil spectra of dipole-interacting DM. We conclude in Sec. 5 and delegate the loop calculation details to the appendix.

2 Framework

2.1 Effective interactions of DM

We start with the most general four-fermion interactions of Dirac DM (χ) and SM fermions (f):

$$\mathcal{L} \supset G_F \sum_a \bar{\chi} \Gamma^a \chi \bar{f} \Gamma^a (\epsilon_a + \tilde{\epsilon}_a i_a \gamma^5) f, \quad (2.1)$$

where the Γ^a matrices (with $a = S, P, V, A, T$) span all the 16 possible independent combinations of Dirac matrices:

$$\Gamma^S = I, \quad \Gamma^P = i\gamma^5, \quad \Gamma^V = \gamma^\mu, \quad \Gamma^A = \gamma^\mu \gamma^5, \quad \Gamma^T = \sigma^{\mu\nu}. \quad (2.2)$$

We refer to the above five possible bi-linear products of Dirac spinors as scalar, pseudo-scalar, vector, axial-vector, and tensor interactions. In Eq. (2.1), we have normalized the interaction strength by the Fermi constant G_F since in the WIMP paradigm, the interactions are typically of this magnitude. Potential deviations are absorbed into the dimensionless constants ϵ_a and $\tilde{\epsilon}_a$. Note that in Eq. (2.1) we have inserted an i_a factor, which is defined as $i_{S,P,T} = i$ and $i_{V,A} = 1$, so that the various terms are hermitian, with ϵ_a and $\tilde{\epsilon}_a$ real numbers—for further discussions see e.g. Refs. [33, 34]. For tensor interactions, one could consider adding γ^5 between $\bar{\chi}$ and χ but the operator $\bar{\chi} \sigma^{\mu\nu} \gamma^5 \chi \bar{f} \sigma_{\mu\nu} f$ is actually identical³ to $\bar{\chi} \sigma^{\mu\nu} \chi \bar{f} \sigma_{\mu\nu} \gamma^5 f$. Hence Eq. (2.1) provides a complete description of all possible Lorentz-invariant four-fermion interactions. This set of effective operators has also been frequently used for DM searches at colliders—see e.g. Ref. [35]. Note importantly that

³This can be seen as follows. In the chiral basis, one can expand it as $\bar{\chi} \sigma^{\mu\nu} \gamma^5 \chi \bar{f} \sigma_{\mu\nu} f = (-\bar{\chi}_R \sigma^{\mu\nu} \chi_L + \bar{\chi}_L \sigma^{\mu\nu} \chi_R) (\bar{f}_R \sigma_{\mu\nu} f_L + \bar{f}_L \sigma_{\mu\nu} f_R)$. Since the cross terms vanish (according to Fierz transformations), $\bar{\chi}_R \sigma^{\mu\nu} \chi_L \bar{f}_L \sigma_{\mu\nu} f_R = \bar{\chi}_L \sigma^{\mu\nu} \chi_R \bar{f}_R \sigma_{\mu\nu} f_L = 0$, the remaining terms imply $\bar{\chi} \sigma^{\mu\nu} \gamma^5 \chi \bar{f} \sigma_{\mu\nu} f = \bar{\chi} \sigma^{\mu\nu} \chi \bar{f} \sigma_{\mu\nu} \gamma^5 f$.

the S , P and T operators are not SM gauge invariant, but could be generated through electroweak symmetry breaking, see the discussion in Sec. 3.2.

In the SM fermion chiral basis, one can also write Eq. (2.1) as

$$\begin{aligned} \mathcal{L} \supset G_F [& \epsilon_S^L \bar{\chi} \chi \bar{f}_R f_L + \epsilon_P^L \bar{\chi} i \gamma^5 \chi \bar{f}_R f_L \\ & + \epsilon_V^L \bar{\chi} \gamma^\mu \chi \bar{f}_L \gamma_\mu f_L + \epsilon_A^L \bar{\chi} \gamma^\mu \gamma^5 \chi \bar{f}_L \gamma_\mu f_L \\ & + \epsilon_T^L \bar{\chi} \sigma^{\mu\nu} \chi \bar{f}_R \sigma_{\mu\nu} f_L + (L \leftrightarrow R)], \end{aligned} \quad (2.3)$$

where $f_{L,R} \equiv P_{L,R} f$, $P_{L,R} \equiv (1 \mp \gamma^5)/2$, ϵ_a^L and ϵ_a^R are linear combinations of ϵ_a and $\tilde{\epsilon}_a$. Given the chiral structure of the SM, and the fact that most results are symmetric under $L \leftrightarrow R$, in this work we will adopt the chiral basis. Note that while ϵ_a and $\tilde{\epsilon}_a$ in Eq. (2.1) are real and independent of each other, ϵ_a^L and ϵ_a^R in the chiral basis are either complex conjugate of each other ($\epsilon_S^R = \epsilon_S^{L*}$, $\epsilon_P^R = \epsilon_P^{L*}$, $\epsilon_T^R = \epsilon_T^{L*}$), or real and independent ($\epsilon_V^R = \text{Re}[\epsilon_V^L]$, $\epsilon_V^L = \text{Re}[\epsilon_V^R]$, $\epsilon_A^R = \text{Re}[\epsilon_A^L]$, $\epsilon_A^L = \text{Re}[\epsilon_A^R]$). Hence the full set of ϵ 's in the chiral basis still contains 10 real independent parameters.

2.2 DM relic abundance

The relic abundance of χ via the standard freeze-out mechanism is approximately given by (see e.g. [36])

$$\Omega_\chi h^2 \simeq 0.12 \frac{x_{\text{f.o.}} \sqrt{g_\star} 1.7 \times 10^{-9} \text{GeV}^{-2}}{23 \cdot 10 \langle \sigma v \rangle}, \quad (2.4)$$

where $x_{\text{f.o.}} \equiv T_{\text{f.o.}}/m_\chi$ is the ratio of the freeze-out temperature $T_{\text{f.o.}}$ to the WIMP mass m_χ ; g_\star is the effective number of relativistic degrees of freedom in the thermal bath at freeze-out; and $\langle \sigma v \rangle$ is defined as [37, 38]

$$\langle \sigma v \rangle \equiv n_{\text{EQ}}^{-2} \int |\mathcal{M}|^2 d\Pi_1 d\Pi_2 d\Pi_3 d\Pi_4 (2\pi)^4 \delta^4 f_1 f_2, \quad (2.5)$$

$$n_{\text{EQ}} \equiv \int 2E_1 d\Pi_1 f_1, \quad d\Pi_i \equiv \frac{g_i d^3 \mathbf{p}_i}{(2\pi)^3 2E_i}. \quad (2.6)$$

Here subscripts 1, 2, \dots , and 4 denote quantities of the first, second, \dots , and the fourth particles in $\chi + \bar{\chi} \rightarrow f + \bar{f}$; δ^4 is short for $\delta^4(p_1 + p_2 - p_3 - p_4)$; and f_1 (f_2) is the thermal distribution function of χ ($\bar{\chi}$). The squared amplitudes $|\mathcal{M}|^2$ has been evaluated and summarized in Tab. 1.

For P , V , T interactions, the annihilation amplitudes are of the s-wave type and consequently are nearly constant in the non-relativistic regime. In this case, we can neglect the velocity dependence and reduce Eq. (2.5) to

$$\langle \sigma v \rangle \equiv \frac{1}{4m_\chi^2} \int |\mathcal{M}|^2 d\Pi_3 d\Pi_4 (2\pi)^4 \delta^4 = \frac{|\mathcal{M}|^2}{32\pi m_\chi^2}. \quad (2.7)$$

For S and A interactions, we have $|\mathcal{M}|^2 \propto v^2$ (p -wave annihilation) and hence the integration is somewhat more complicated. Assuming Maxwell-Boltzmann distributions for f_1 and f_2 , Eq. (2.5) can be reduced to [38]

$$\langle \sigma v \rangle \equiv \frac{1}{8m_\chi^4 T K_2^2(m_\chi/T)} \int_{4m_\chi^2}^{\infty} \sigma \sqrt{s} (s - 4m_\chi^2) K_1(\sqrt{s}/T) ds. \quad (2.8)$$

Table 1. Annihilation amplitudes ($|\mathcal{M}|^2$), cross sections (σ), thermally averaged cross sections ($\langle\sigma v\rangle$), and benchmark values of ϵ_a^* used in Eq. (2.11) for the five types of effective interactions. We neglected the mass of the final states and assume that the annihilating DM particles are non-relativistic with v being their relative velocity. The results have been expanded in v and only leading-order terms are retained. Results for ϵ_a^R and ϵ_a^L are identical.

	S	P	V	A	T
$ \mathcal{M} ^2 / \left G_F m_\chi^2 \epsilon_a^{L,R} \right ^2$	$2v^2$	8	16	$2v^2(1 + \cos^2 \theta)$	32
$\sigma / \left G_F m_\chi^2 \epsilon_a^{L,R} \right ^2$	$\frac{v}{4\pi s}$	$\frac{1}{\pi s v}$	$\frac{2}{\pi s v}$	$\frac{v}{3\pi s}$	$\frac{4}{\pi s v}$
$\langle\sigma v\rangle / \left G_F m_\chi^2 \epsilon_a^{L,R} \right ^2$	$\frac{3}{8\pi} T m_\chi^{-3}$	$\frac{1}{4\pi} m_\chi^{-2}$	$\frac{1}{2\pi} m_\chi^{-2}$	$\frac{1}{2\pi} T m_\chi^{-3}$	$\frac{1}{\pi} m_\chi^{-2}$
ϵ_a^*	0.49	0.13	0.089	0.43	0.063

Here K_1 and K_2 are K -type Bessel function of orders 1 and 2, $s = (p_1 + p_2)^2 = 4m_\chi^2 + m_\chi^2 v^2$, and σ is the total annihilation cross section [39]:

$$\sigma = \int \frac{|\mathcal{M}|^2}{16\pi s (s - 4m_\chi^2)} dq^2, \quad (2.9)$$

where $q^2 = (p_3 - p_1)^2 \approx -m_\chi^2(1 - v \cos \theta)$, with θ the angle between \mathbf{p}_1 and \mathbf{p}_3 . Integrating q^2 from $-m_\chi^2(1 + v)$ to $-m_\chi^2(1 - v)$, we obtain results for σ that are given in Tab. 1.

Plugging the results for σ into Eq. (2.8) with $v \rightarrow m_\chi^{-1} \sqrt{s - 4m_\chi^2}$, we can integrate Eq. (2.8) analytically by noticing that for any value of $p > -1$,

$$\int_{4m^2}^{\infty} (s - 4m^2)^p K_1(\sqrt{s}/T) \frac{1}{\sqrt{s}} ds = 2^{1+2p} T (mT)^p K_p(2m/T) \Gamma(1 + p), \quad (2.10)$$

where Γ is the Euler gamma function. The results for $\langle\sigma v\rangle$ are then expanded in T/m and summarized in Tab. 1.

Using the results for $\langle\sigma v\rangle$ with $T_{f.o} \simeq m_\chi/23$ (the typical freeze-out temperature) in Eq. (2.4), we obtain

$$\Omega_\chi h^2 \simeq 0.12 \left(\frac{100 \text{ GeV}}{m_\chi} \right)^2 \left| \frac{\epsilon_a^*}{\epsilon_a^{L,R}} \right|^2, \quad (2.11)$$

where ϵ_a^* denotes benchmark values: $\epsilon_S^* = 0.49$, $\epsilon_P^* = 0.13$, $\epsilon_V^* = 0.089$, $\epsilon_A^* = 0.43$, and $\epsilon_T^* = 0.063$. Note that ϵ_a^* for $a = S$ or A is generally larger than for other cases because the cross section is velocity suppressed, which implies that they would freeze out at higher temperatures for the same coupling strength. Hence to reach the same relic abundance (i.e. same freeze out temperature), the coupling needs to be larger.

3 Loop-induced electromagnetic interactions

3.1 Closing the loop

In the presence of any of the $\bar{\chi}\text{-}\chi\text{-}\bar{f}\text{-}f$ interactions formulated in Eq. (2.1) or Eq. (2.3), we can close the fermion lines of f and attach a photon external line, as illustrated in Fig. 1.

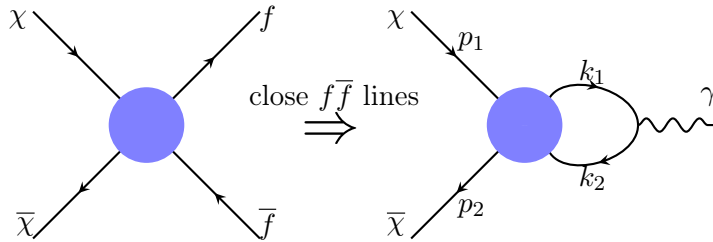


Figure 1. Loop-induced electromagnetic interactions. In the presence of effective $\bar{\chi}\text{-}\chi\text{-}\bar{f}\text{-}f$ interactions where χ is a DM fermion and f is a SM fermion, the f and \bar{f} lines can be closed to form a loop diagram, which after attaching a photon line can generate electric and/or magnetic dipoles of DM.

This generally leads to loop-induced electromagnetic interactions of χ .

Closing the loop in this way one gets amplitudes which take the general form

$$\begin{aligned}
 i\mathcal{M}_{\text{loop}} &= i\bar{u}_2\Gamma^a u_1 \int \frac{d^4k}{(2\pi)^4} \text{tr} \left[\frac{1}{\not{k}_2 - m_f} i e Q_f \gamma^\mu \frac{1}{\not{k}_1 - m_f} \tilde{\Gamma}^a \right] \varepsilon_\mu G_X(p_1, p_2, k_1, k_2) \\
 &\equiv i\bar{u}_2 \mathcal{F}^\mu u_1 \varepsilon_\mu,
 \end{aligned} \tag{3.1}$$

where \bar{u}_2 , u_1 , ε_μ represent the three external lines; the momenta p 's and k 's have been defined in Fig. 1 with $k = p_1 - k_1 = p_2 - k_2$; m_f and Q_f are the mass and the electric charge of f ; $\tilde{\Gamma}^a \equiv \Gamma^a P_{L,R}$; G_X is the coefficient of the effective operator considered. The most general form of the \mathcal{F}^μ vertex function that respects Lorentz and electromagnetic gauge invariance can be decomposed as a combination of four terms, each one with its own form factor (see e.g. [40, 41]):

$$\mathcal{F}^\mu = \mathcal{F}_Q(q^2)\gamma^\mu + \mathcal{F}_M(q^2)i\sigma^{\mu\nu}q_\nu + \mathcal{F}_E(q^2)\sigma^{\mu\nu}\gamma^5 q_\nu + \mathcal{F}_A(q^2)(q^2\gamma_\mu - q_\mu\not{q})\gamma^5. \tag{3.2}$$

Here $q \equiv p_1 - p_2$ and in the limit of $q^2 \rightarrow 0$, the four form factors $\mathcal{F}_Q(0)$, $\mathcal{F}_M(0)$, $\mathcal{F}_E(0)$, and $\mathcal{F}_A(0)$ are the electric charge, magnetic dipole, electric dipole and anapole of χ , respectively. For simplicity, we denote

$$d_M \equiv \mathcal{F}_M(0), \quad d_E \equiv \mathcal{F}_E(0). \tag{3.3}$$

In this work, we do not consider the electric charge and anapole of χ because the former remains zero at loop levels if DM is electrically neutral at tree level and the latter causes suppressed signals in DM direct detection. This suppression can be seen from the form of the \mathcal{F}_A term of Eq. (3.2), which in the low- q^2 regime is proportional to q^2 . This $\mathcal{O}(q^2)$ coefficient will be canceled by the photon propagator which is proportional to $\mathcal{O}(q^{-2})$. Indeed, Ref. [28] has shown that the effect of anapole in direct detection is nearly equivalent to that of contact interactions. Thus, unlike with dipoles, the direct detection does not profit from the several orders of magnitude enhancement related to the $1/q^2$ behavior of the amplitude, see below. Neutral χ might possess a non-vanishing charge radius defined as $d\mathcal{F}_Q(q^2)/dq^2|_{q^2 \rightarrow 0}$. Its effect in direct detection is also suppressed for the same reason.⁴

⁴For a scalar DM candidate the coupling to the photon that could be loop induced from an effective

Table 2. Electromagnetic dipoles generated by the loop diagram in Fig. 1. Here the “ t ” and “ s ” indices refer to the results obtained considering the corresponding channel in Eq. (3.4). $C^{(t)}$ and $C^{(s)}$ are given in Eq. (3.5).

	S	P	V	A	T
$d_M^{(t)} / \left(\frac{eQ_f G_F}{16\pi^2} \right)$	$(\epsilon_S^L + \epsilon_S^R)m_f$	0	$\frac{1}{3}(\epsilon_V^L + \epsilon_V^R)m_\chi$	$-(\epsilon_A^L - \epsilon_A^R)m_\chi$	$4(\epsilon_T^L + \epsilon_T^R)m_f C^{(t)}$
$d_E^{(t)} / \left(\frac{eQ_f G_F}{16\pi^2} \right)$	0	$(\epsilon_P^L + \epsilon_P^R)m_f$	0	0	$4i(\epsilon_T^L - \epsilon_T^R)m_f C^{(t)}$
$d_M^{(s)} / \left(\frac{eQ_f G_F}{16\pi^2} \right)$	0	0	0	0	$4(\epsilon_T^L + \epsilon_T^R)m_f C^{(s)}$
$d_E^{(s)} / \left(\frac{eQ_f G_F}{16\pi^2} \right)$	0	0	0	0	$4i(\epsilon_T^L - \epsilon_T^R)m_f C^{(s)}$

Since they involve a loop where momenta runs from 0 to infinity, the use of the effective theory to compute these dipoles does not necessarily lead to consistent results. Related to that, two explicit UV complete theories leading to the same operators at low energy does not necessarily lead to the same dipoles. Explicit calculations shows that indeed the calculation of the dipoles from Fig. 1, i.e. with G_X a constant, is not consistent, since it leads to loop integral divergent results. Thus one must open the four-fermion interactions. Here we will open them along the two simplest possible ways, from the exchange of a t -channel or s -channel heavy mediator giving momentum-dependent G_X functions

$$G_X^{(s)} = \frac{y^2}{s - m_{\text{med}}^2}, \quad G_X^{(t)} = \frac{y^2}{t - m_{\text{med}}^2}, \quad (3.4)$$

where m_{med} and y are the mediator mass and coupling, $s = (p_1 - p_2)^2$ and $t = (p_1 - k_1)^2$.⁵ There could be more complex scenarios for the internal structure of the effective vertex, where e.g. G_X is generated by a box diagram, for which the current framework does not apply since it typically requires two-loop calculations (which are beyond the scope of this work).

Substituting Eq. (3.4) in Eq. (3.1) and performing the loop integration (see Appendix A), we obtain the results in Tab. 2 where $C^{(t)}$ and $C^{(s)}$ in the last column are defined as

$$C^{(t)} \equiv 1 + \log(m_f^2/m_{\text{med}}^2), \quad C^{(s)} \equiv \frac{1}{\varepsilon} + \log(\mu^2/m_f^2). \quad (3.5)$$

Here $C^{(t)}$ is finite but $C^{(s)}$ contains a UV divergence, with μ and ε defined by the dimensional regularization $d^4k/(2\pi)^4 \rightarrow \mu^{2\varepsilon} d^{4-2\varepsilon}k/(2\pi)^{4-2\varepsilon}$.⁶ The results are obtained assuming

operator (i.e. $\phi_{DM}^\dagger \phi_{DM} \bar{f} f$ or $\phi_{DM}^\dagger \phi_{DM} \bar{f} \gamma_5 f$), coupling it in pairs to a pair of charged fermions, would lead to suppressed direct detection in a similar way, as it would induce only a charged radius. For a Majorana DM candidate, as is well known, dipole interactions identically vanish, and an anapole leads to suppressed direct detection in a similar way than for a Dirac fermion.

⁵Note that when the left diagram is interpreted as DM annihilation, we flip the direction of p_2 and obtain $s = (p_1 + p_2)^2$ which is the conventional definition of s as the Mandelstam variable.

⁶Note however that the tensor operator cannot result from a simple tree level s -channel exchange, but must be induced e.g. from a loop diagram coupling the s -channel mediator to the pair of DM particles and from another loop diagram coupling the s -channel mediator to the pair of SM fermions. This case is thus of

the heavy mediator limit: $m_{\text{med}} \gg m_{\chi,f}$. It is noteworthy that the loop-induced dipoles for the S , P and T cases are proportional to m_f while for the other two cases they are proportional to m_χ . This is due to the well-known chirality-flipping nature of S , P , T interactions—see discussions in Ref. [42].

For the t -channel case a magnetic or an electric dipole is always induced (even if never both), depending on the operator considered. In all cases this allows non-suppressed direct detection signals as we will see below. Barring cancellations this implies that any UV complete model generating any one of these operators through a t -channel transition can be efficiently probed via direct detection, see below. This is presumably also the case for models where the effective interactions would be induced at loop level, such as through box diagrams (but we will not explicitly check this statement here). Note that for this t -channel case all the results are obtained finite as it should obviously be. In the s -channel case instead no dipoles at all are obtained for the S , P , V and A cases, as a result of the fact that in this case the loop is a self-energy which cannot give rise to a $\sigma_{\mu\nu}$. For the tensor case one can get a dipole as the effective operator already contain a $\sigma_{\mu\nu}$ to start with.

In summary, we get two general classes of scenarios, the one leading for simple reasons to vanishing dipoles and the ones leading to non-vanishing dipoles. For the second class we have

$$d_{M,E} = \frac{eQ_f G_F}{16\pi^2} \times \mathcal{O}(\epsilon_a) \times \begin{cases} m_\chi & \text{for } a = V, A \\ m_f & \text{for } a = S, P, T \end{cases}, \quad (3.6)$$

where the $\mathcal{O}(\epsilon_a)$ part has been specified in Tab. 2.

3.2 A UV complete example

The results obtained above for the dipoles by replacing in Fig. 1 the four fermion interaction by a t -channel propagator have no reasons to give exactly what we would get in a UV complete model leading to these operators through a t -channel heavy mediator exchange. Since DM is neutral and the SM fermions are charged, the t -channel heavy mediator has necessarily a non-vanishing electric charge. Thus in a UV complete model there are necessarily extra diagrams that may modify the dipoles, simply attaching the photon to the heavy mediator rather than to the SM charged fermion. However, for a mediator much heavier than the other particles we do not expect in general that these extra diagrams could induce any large destructive interference for the dipole induced (given in particular the chiral structure of the SM), or even largely change the results. To illustrate this, we consider a simple UV complete model leading to the 4-fermion interactions through t -channel exchange. Consider a charged scalar ϕ^\pm that couples to f_R and χ :

$$\mathcal{L} \supset y \bar{\chi} f_R \phi^+ + \text{h.c.} \quad (3.7)$$

limited interest. Tensor interactions are generated in an easier way from tree level t -channel (through Fierz transformation) or one loop box diagrams. Thus, even if this divergence, that we get only for this s -channel tensor case, means that the result is inconsistent (and that in UV complete models this dipole interaction necessarily never comes without other interactions), we will not elaborate more on this problem. At a very rough level one can expect constraints on this case similar to the ones obtained below for the t -channel T case.

Assuming the scalar boson mass m_ϕ is heavy, by integrating out ϕ^\pm , we obtain the effective interaction

$$\mathcal{L}_{\text{eff}} = -G_X \bar{\chi} P_R f \bar{f} P_L \chi, \quad (3.8)$$

where $G_X = yy^*/m_\phi^2$. One can reformulate it to the form in Eq. (2.1) via Fierz transformation:⁷

$$\mathcal{L}_{\text{eff}} = \frac{1}{4} G_X \bar{\chi} \gamma^\mu \chi \bar{f}_R \gamma_\mu f_R - \frac{1}{4} G_X \bar{\chi} \gamma^\mu \gamma^5 \chi \bar{f}_R \gamma_\mu f_R. \quad (3.9)$$

Eq. (3.9) contains two types (V and A) of effective interactions, with the following ϵ 's:⁸

$$\begin{aligned} \epsilon_V^L &= 0, \quad \epsilon_V^R = \frac{1}{4} G_X / G_F, \\ \epsilon_A^L &= 0, \quad \epsilon_A^R = -\frac{1}{4} G_X / G_F. \end{aligned} \quad (3.10)$$

According to Tab. 2, by summing up the contributions of the above ϵ 's, i.e. from Eq. (3.9) and Tab. 2, we obtain the magnetic dipole in the EFT approach:

$$d_M^{\text{EFT}} = -\frac{1}{6} m_\chi \cdot \frac{e G_X Q_f}{16\pi^2}. \quad (3.11)$$

One can also compute exactly the dipoles directly from the model Lagrangian. As already mentioned above, there are two diagrams that couple $\chi\text{-}\bar{\chi}$ to the photon, one with the photon coupled to f and the other one with the photon coupled to ϕ^\pm . The resulting magnetic dipole from the two diagrams reads (see Appendix A for details on this calculation):

$$d_M^{\text{UV}} = -\frac{1}{4} m_\chi \cdot \frac{e G_X Q_f}{16\pi^2}. \quad (3.12)$$

Note that a purely left-handed interaction involving a SM fermion doublet and a scalar doublet instead of f_R and ϕ^+ in Eq. (3.7) gives the same dipoles as the purely right-handed case of Eq. (3.7).

By comparing Eq. (3.12) to Eq. (3.11), we see that the magnetic dipole computed in the UV theory is actually 50% higher than the EFT result. Therefore, when using the results of Tab. 2, one should keep in mind that the results may be changed due to new contributions in complete theories. Nevertheless, the EFT driven results of Tab. 2 provide correct estimates of the order of magnitude of the dipoles. In other words, one cannot exclude that specific UV models would give quite different results between both approaches but this explicit example shows that in simple frameworks this is not the case.

⁷See, e.g., Ref. [43], page 65.

⁸It is not surprising that we get a combination of the SM gauge group invariant V and A operators since the original interactions of Eqs. (3.7) and (3.8) are gauge invariant. Operators of the S , P or T type can be generated in UV complete models, for instance from inducing a gauge invariant dimension 7 operator involving an extra Higgs doublet and electroweak symmetry breaking. In this case the extra interactions involving the Higgs doublet components rather than the Higgs boson vev do not induce an extra contribution to the dipole at same one loop order (but could be relevant for DM annihilation for multi-TeV DM, i.e. for $m_{DM} \gg v_{EW}$). Such operators could also be generated if for instance, on top of the interaction of Eq. (3.7), there exists a similar interaction involving a SM left-handed doublet and a scalar doublet rather than f_R and ϕ^+ , and if the charged component of this scalar doublet mixes with ϕ^+ via electroweak symmetry breaking.

3.3 Expected magnitude of electromagnetic dipoles

The relic abundance constraint, $\Omega_\chi h^2 \simeq 0.12$, requires that the ϵ coefficients of the effective operators are typically of the order of a few (or tens of) percent—see Tab. 1 and Eq. (2.11). By requiring that $\Omega_\chi h^2 \simeq 0.12$ is correctly produced, according to Eq. (2.11), we replace $\epsilon_a^{L,R}$ in Tab. 2 with $100 \text{ GeV} \cdot m_\chi^{-1} \epsilon_a^*$ and obtain

$$|d_M^{(t)}| \approx \begin{cases} 4.3 \times 10^{-21} |Q_f| \text{ ecm} & \text{for } a = V \\ 6.2 \times 10^{-20} |Q_f| \text{ ecm} & \text{for } a = A \end{cases}, \quad (3.13)$$

where $\text{ecm} \equiv e \times \text{cm} \approx 15350.3 \text{ eV}^{-1}$ is a commonly used unit for electromagnetic dipoles. The result is almost independent of m_χ and m_f . It only depends on the electric charge of the SM fermion involved, Q_f , which can be $2/3$ (for $f = u, c, t$), $-1/3$ (for $f = d, s, b$), or -1 (for $f = e, \mu, \tau$).

For S , P , and T interactions, the dipoles depend on m_f . Since in this work we require that $\chi\bar{\chi} \rightarrow f\bar{f}$ is responsible for the relic abundance, we concentrate on cases with $m_\chi \gtrsim m_f$. With this assumption, one can still apply $\epsilon_a^{L/R} = 100 \text{ GeV} \cdot m_\chi^{-1} \epsilon_a^*$ to the remaining dipoles:

$$|d_M^{(t)}| \approx 7.2 \times 10^{-20} |Q_f| \frac{m_f}{m_\chi} \text{ ecm}, \quad \text{for } a = S, \quad (3.14)$$

$$|d_E^{(t)}| \approx 1.8 \times 10^{-20} |Q_f| \frac{m_f}{m_\chi} \text{ ecm}, \quad \text{for } a = P, \quad (3.15)$$

$$|d_{E,M}^{(t)}| \approx 3.7 \times 10^{-20} |Q_f| \frac{m_f}{m_\chi} \text{ ecm}, \quad \text{for } a = T. \quad (3.16)$$

4 Electromagnetic dipoles in direct detection

In direct detection experiments, the differential event rate of DM-nucleus scattering⁹ can be evaluated via (see e.g. [39, 44]):

$$\frac{dR}{dE_r} = N_T n_\chi \epsilon(E_r) \int \frac{d\sigma}{dE_r} v f_\oplus(\mathbf{v}) \Theta(v - v_{\min}) d^3\mathbf{v}. \quad (4.1)$$

Here E_r is the nuclear recoil energy; N_T is the total number of target nuclei; n_χ is the local DM number density; $\epsilon(E_r)$ is the detection efficiency; $\frac{d\sigma}{dE_r}$ is the differential cross section; $f_\oplus(\mathbf{v})$ is the DM velocity distribution in the Earth frame; v_{\min} is the minimal velocity to generate a given E_r ,

$$v_{\min} = \sqrt{\frac{m_N E_r}{2\mu_{\chi N}^2}}, \quad (4.2)$$

where m_N is the nucleus mass and $\mu_{\chi N} \equiv m_\chi m_N / (m_\chi + m_N)$ is the DM-nucleus reduced mass. For the local DM density we take $n_\chi = \rho_\chi / m_\chi$ and $\rho_\chi = 0.4 \text{ GeV}/\text{cm}^3$ [45].

The DM velocity distribution $f_\oplus(\mathbf{v})$ is often parametrized by a truncated Maxwellian distribution in the frame of the Galaxy and then boosted to the Earth frame. The specific

⁹In Ref. [16], it was pointed out for leptophilic DM that DM-nucleus scattering largely dominates over DM-electron scattering (for DM masses beyond GeV) and this is expected here too for the same reasons.

form reads

$$f_{\oplus}(\mathbf{v}) = \frac{1}{N_f} \exp\left[-\frac{\tilde{v}^2}{v_0^2}\right] \Theta(v_{\text{esc}} - \tilde{v}), \quad (4.3)$$

where $\tilde{v} = |\mathbf{v} + \mathbf{v}_{\oplus}|$ and $|\mathbf{v}_{\oplus}| \approx 240$ km/s is the velocity of the Earth with respect to the Galaxy; $v_{\text{esc}} \approx 550$ km/s is the escape velocity of the Galaxy; $v_0 = 220$ km/s is the mean velocity of the Maxwellian distribution. The N_f factor normalizes f_{\oplus} so that $\int f_{\oplus}(\mathbf{v}) d^3\mathbf{v} = 1$:

$$N_f = \pi^{3/2} v_0^3 \left[\text{erf}\left(\frac{v_{\text{esc}}}{v_0}\right) - \frac{2}{\sqrt{\pi}} \frac{v_{\text{esc}}}{v_0} \exp\left(-\frac{v_{\text{esc}}^2}{v_0^2}\right) \right]. \quad (4.4)$$

The differential cross sections for DM-nucleus scattering via dipoles read [17, 21]:

$$\frac{d\sigma_M}{dE_r} \approx d_M^2 \frac{\alpha Z^2 F_E^2}{E_r} \left[1 - \frac{E_r}{2m_N v^2} \left(1 + 2\frac{m_N}{m_\chi} \right) \right] + d_M^2 \frac{\alpha G F_M^2}{2m_N v^2}, \quad (4.5)$$

$$\frac{d\sigma_E}{dE_r} \approx d_E^2 \frac{\alpha Z^2}{E_r v^2} F_E^2. \quad (4.6)$$

Note the $1/E_r$ dependence of these differential cross sections, stemming from the propagator of the (massless) photon. As compared to a standard WIMP case, where the particle exchanged with the nucleon has typically an electroweak scale mass, this will largely boost the number of events in direct detection events, since the recoil energy considered in these experiments is typically of order 5-50 keV (see below). This explains why below the constraints from direct detection through dipoles will be competitive, despite the fact that they involve loop suppressed quantities.

In Eqs. (4.5)-(4.6), $\alpha = 1/137$, Z is the atomic number, F_E and F_M are two nuclear form factors, and G is a dimensionless quantity depending on the nuclear spin J and the nuclear magnetic dipole d_N [17]:

$$G = \frac{2(J+1)}{3J} \left(\frac{d_N A}{d_n} \right)^2 \approx 7256.78 \text{ (for Xe)}, \quad (4.7)$$

where $d_n = e/(2m_p)$ is the nuclear magneton, and A is the mass number. For the nuclear form factors, we adopt the following approximate expressions [17]:

$$F_E = 3 \left[\frac{\sin(qr) - qr \cos(qr)}{(qr)^3} \right] e^{-q^2 s^2}, \quad (4.8)$$

$$F_M = \frac{\sin(q\tilde{r})}{q\tilde{r}} \Theta(q\tilde{r} < 2.55) + 0.21 \Theta(2.55 < q\tilde{r} < 4.5), \quad (4.9)$$

where $r = 1.12A^{1/3}$ fm, $\tilde{r} = A^{1/3}$ fm, $s = 1$ fm, and $q = \sqrt{2E_r m_N}$. The Θ function takes either the value 1 or the value 0, depending on whether the condition it involves is satisfied. For Xe targets, $q\tilde{r} < 4.5$ corresponds to $E_r < 117$ keV, which in practice is always satisfied.

In the magnetic dipole cross section (4.5) we have included both SI ($\propto F_E^2$) and SD ($\propto F_M^2$) parts because they can be equally important. For example, when $m_\chi = m_N$ and $v = 1.2v_{\text{min}}$, the ratio of the two parts at $E_r = 30$ keV is about 1.6. For the electric

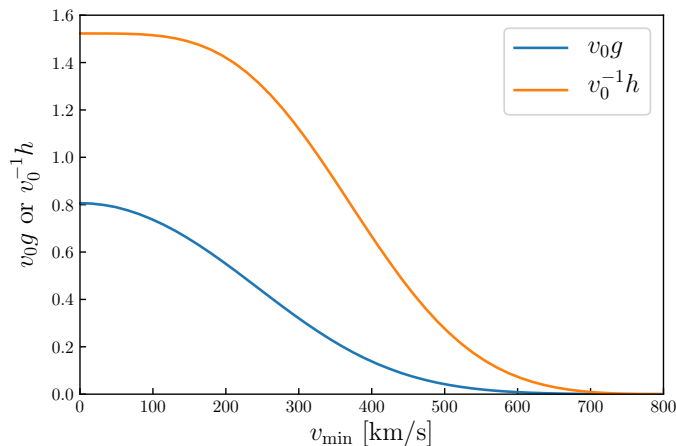


Figure 2. Results of $g(v_{\min})$ and $h(v_{\min})$ in Eqs. (4.12) and (4.13).

dipole cross section (4.6) we have neglected a possible SD contribution because it is highly suppressed. The fundamental reason for this is that electric charges of nucleons can be added coherently, unlike magnetic moments of nucleons. As a consequence, the electric dipole cross section is generally much larger than the magnetic one when $d_M \simeq d_E$.

For both Eqs. (4.5) and (4.6), the velocity dependence can be written as follows:

$$\frac{d\sigma}{dE_r} = \frac{1}{v^2} \left(\frac{d\sigma_g}{dE_r} + v^2 \frac{d\sigma_h}{dE_r} \right), \quad (4.10)$$

where $d\sigma_g/dE_r$ and $d\sigma_h/dE_r$ are velocity independent. Substituting Eq. (4.10) into Eq. (4.1), we obtain

$$\frac{dR}{dE_r} = N_T n_\chi \epsilon(E_r) \left[\frac{d\sigma_g}{dE_r} g(v_{\min}) + \frac{d\sigma_h}{dE_r} h(v_{\min}) \right], \quad (4.11)$$

where

$$g(v_{\min}) \equiv \int v^{-1} f_\oplus(\mathbf{v}) \Theta(v - v_{\min}) d^3\mathbf{v}, \quad (4.12)$$

$$h(v_{\min}) \equiv \int v f_\oplus(\mathbf{v}) \Theta(v - v_{\min}) d^3\mathbf{v}, \quad (4.13)$$

can be computed independently of the cross section and of the kinematics of DM-nucleus scattering. When numerically evaluating the integrals, we take Eq. (4.3) with $\tilde{v} = (v^2 + v_\oplus^2 - 2vv_\oplus \cos\theta)^{1/2}$ where θ is the angle between \mathbf{v}_\oplus and \mathbf{v} , and integrate θ from 0 to π , v from 0 to $v_0 + v_{\text{esc}}$. The results are presented in Fig. 2.

Using Eq. (4.11), we plot in Fig. 3 the differential event rates (dashed curves) for $d_M = 5 \times 10^{-20}$ ecm, $d_E = 1 \times 10^{-22}$ ecm, assuming $m_\chi = 100$ GeV and a 10^3 kg liquid Xe target. For comparison, we also present a curve for the following SI contact-interacting cross section:

$$\frac{d\sigma_{\text{contact}}}{dE_r} = \sigma_n \frac{m_N A^2 F_E^2}{2\mu_{\chi n}^2 v^2}, \quad (4.14)$$

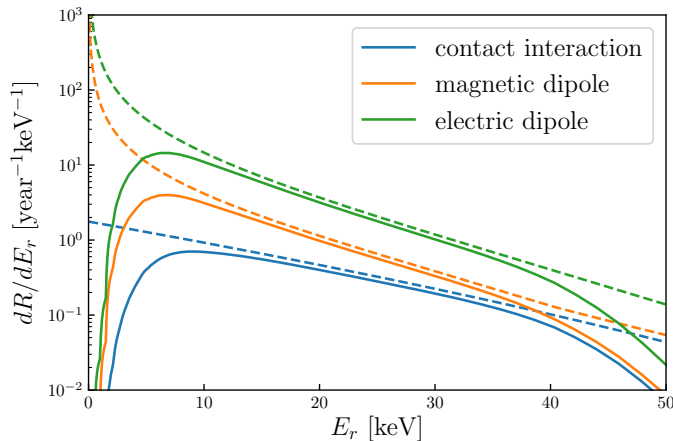


Figure 3. Event rates for DM-nucleus scattering via magnetic and electric dipoles compared with the standard (contact-interaction) case. Shown examples take $d_M = 5 \times 10^{-20}$ ecm, $d_E = 1 \times 10^{-22}$ ecm, $\sigma_n = 10^{-46}$ cm², and $m_\chi = 100$ GeV. Dashed curves assume ideal detection efficiency and solid curves take the XENON-1T detection efficiency [10] into account.

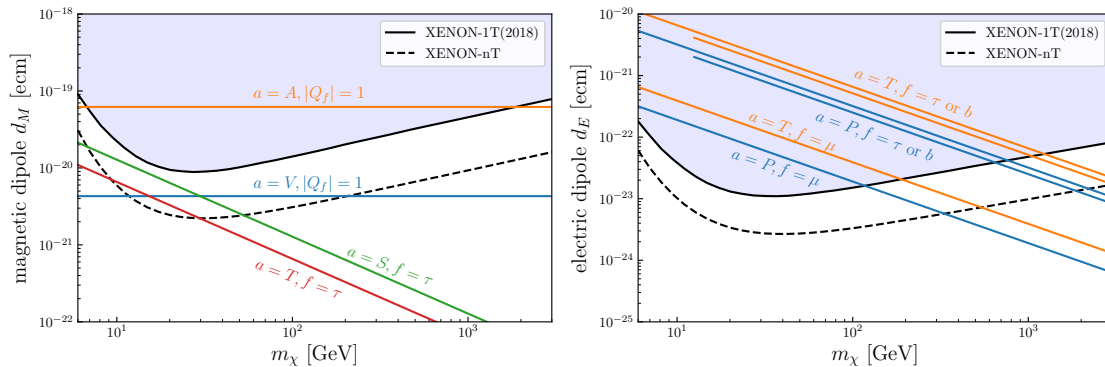


Figure 4. The loop-induced magnetic dipole d_M (left panel) and electric dipole d_E compared with the XENON-1T [10] limit and the future XENON-nT [46] sensitivity. The theoretical expectations of d_M and d_E are computed according to Eqs. (3.13)-(3.16). Dipoles for other fermions than the ones considered in these panels can be obtained for example from the τ case from a simple multiplication by Q_f/Q_τ for V and A and by $Q_f m_f/(Q_\tau m_\tau)$ for S , P and T .

where $\mu_{\chi n} = m_\chi m_n/(m_\chi + m_n)$ is the DM-nucleon reduced mass. For the DM-nucleon cross section σ_n we have taken the typical value that can be probed by direct detection experiment today, $\sigma_n = 10^{-46}$ cm². For the solid curves in Fig. 3, we have included the detection efficiency of XENON-1T, which is taken from Fig. 1 in Ref. [10]. The range of relevant recoil energy in direct detection experiments is relatively narrow, as below ~ 5 keV and above ~ 50 keV the efficiency is suppressed (compare dashed and solid lines in Fig. 3). As can be seen in this figure too, within this range, the dipole lines display, as expected, an extra $1/E_r$ dependence with respect to the contact interaction case.

As a result of this relatively narrow range of recoil energy, it is possible to recast the XENON-1T bounds obtained for a contact interaction into bounds holding for the

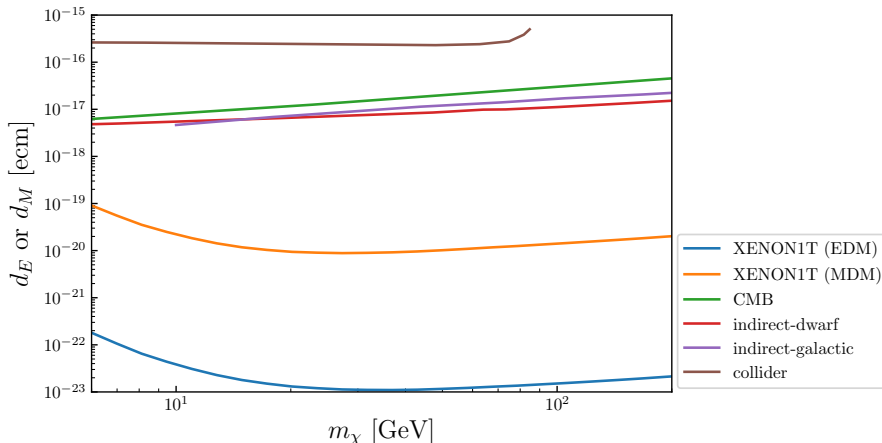


Figure 5. Comparison of direct detection bounds with other known bounds on DM electric/magnetic dipoles. The direct detection bounds (XENON-1T) are the same as those in Fig. 4. The CMB bound is taken from Ref. [21]. The indirect detection bounds, also taken from Ref. [21], are derived from FERMI-LAT constraints on γ -rays from the Galaxy (labelled as indirect-galactic) and its dwarf satellite galaxies (indirect-dwarf). The collider bound is taken from Ref. [20].

massless mediator ($\propto 1/E_r$) case of interest here. To this end, we apply a spectrum-fitting technique previously adopted in Ref. [47], namely using Eq. (4.14) to fit the dipole-interacting recoil spectra. Specifically, for a given set of d_M (d_E) and m_χ , one can correspondingly find values of σ_n and m'_χ (usually different from m_χ) that minimizes the integral $\int (dR_{\text{dipole}}/dE_r - dR_{\text{contact}}/dE_r)^2 dE_r$ where dR_{dipole}/dE_r and dR_{contact}/dE_r are the dipole- and contact-interacting spectra (including the detection efficiency). The minimization is performed under an additional constraint that their total rates are equal. We find that after the minimization, the two spectra are usually very close, with relative differences typically below 20%, which is consistent with the conclusion in Ref. [47]. By mapping d_M (d_E)- m_χ to σ_n - m'_χ and taking the XENON-1T limit from Ref. [10], we obtain the bounds on d_M and d_E , presented in Fig. 4. For comparison, we also show in Fig. 5 other known bounds on DM electromagnetic dipoles from indirect detection, CMB observations, and collider searches. These bounds in the WIMP regime are known to be much weaker than that from direct detection.

Fig. 4 shows that the possibility that the axial operators would be responsible for the observed DM relic density is already excluded by direct detection experiments within the $6.8 \text{ GeV} < m_\chi < 1.9 \text{ TeV}$ range for charged leptons. Future experiments such as XENON-nT will enlarge this range significantly. For the vector case, although it is beyond the current best limit from XENON-1T, future XENON-nT will be able to probe the range $11.8 \text{ GeV} < m_\chi < 205 \text{ GeV}$. The axial case is more constrained than the vector one because it requires a larger coefficient to account for the relic density constraint due to p -wave annihilation, see Eq. (2.11) and Tab. 1. For the S , P and T cases the additional m_f/m_χ dependence of the dipoles decreases the sensitivity for high values of m_χ but boosts it for low values. The sensitivity also splits among generations of fermions. Taking the

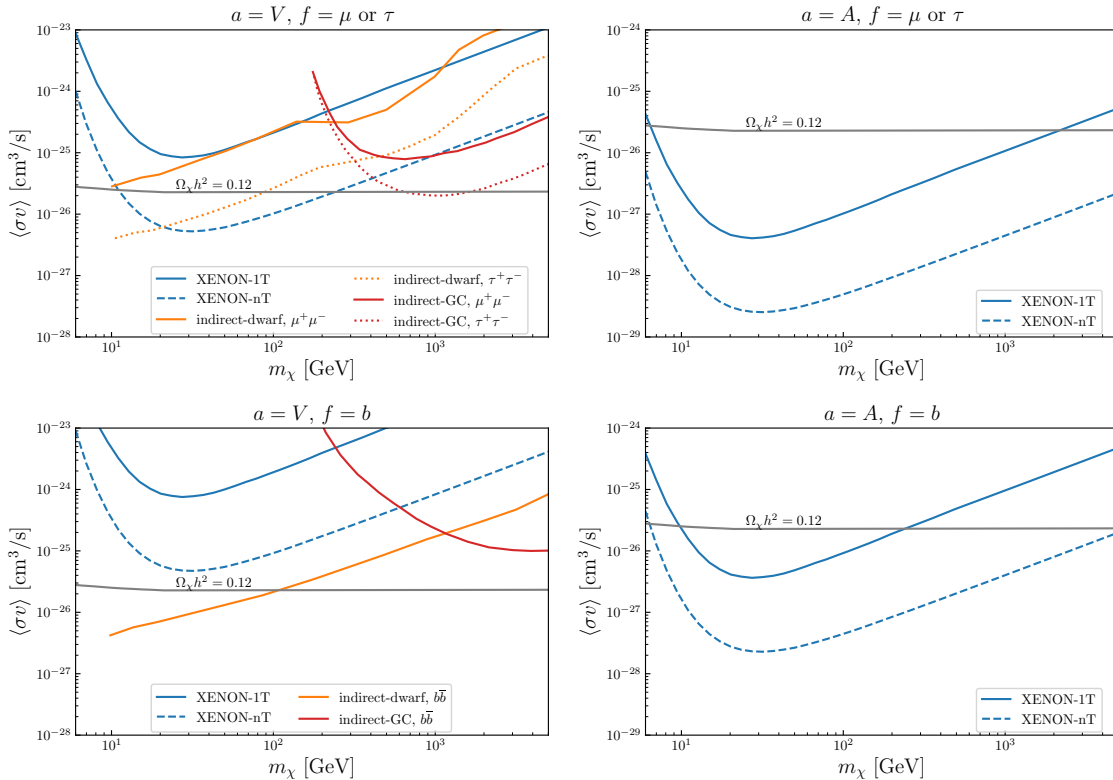


Figure 6. Direct detection bounds on $\langle\sigma v\rangle$ in comparison with indirect detection bounds, both obtained assuming $\Omega_\chi h^2 = 0.12$. For direct detection, we take the XENON-1T/nT bounds on d_M obtained in Fig. 4 and recast them to bounds on ϵ 's according to Tab. 2, and further to bounds on $\langle\sigma v\rangle$ according to Tab. 1, assuming $a = V/A$. For indirect detections, the “indirect-dwarf” bounds are taken from Ref. [48], and “indirect-GC” from [49], assuming that DM annihilates to $\tau^+\tau^-$, $\mu^+\mu^-$ or $b\bar{b}$. The horizontal line shows the thermal cross section value.

tensor case in the right panel of Fig. 4 as an example, XENON-1T has excluded $m_\chi \lesssim 189$ GeV for $f = \mu$ while for $f = \tau$ this bound increases to $m_\chi \lesssim 1.2$ TeV. The future experiment XENON-nT will be able to improve the mass bound by roughly a factor of three.

The four fermion interactions also induce fluxes of cosmic rays from the annihilation into charged fermion they induce today at tree level in the galactic center and dwarf galaxies. Indirect detection experiments give upper bounds on these fluxes which are generally translated into upper bounds on the annihilation cross section assuming $\Omega_\chi h^2 = 0.12$ (i.e. not looking at the implications that this annihilation cross section could have on the relic density). In Fig. 6 we show for the V case how these bounds compare with the bounds that can be obtained on the same cross sections from the bound that direct detection set on the dipoles and thus on the coefficient of the four-fermion operators (assuming $\Omega_\chi h^2 = 0.12$ anyway there too). As Fig. 6 shows, despite that at tree level direct detection experiments are not much sensitive to the four-fermion operators for charged leptons or heavy quarks, when the loop-induced dipoles are taken into account, direct detection offers competitive constraints on such operators in comparison with indirect detection. For the A case (and

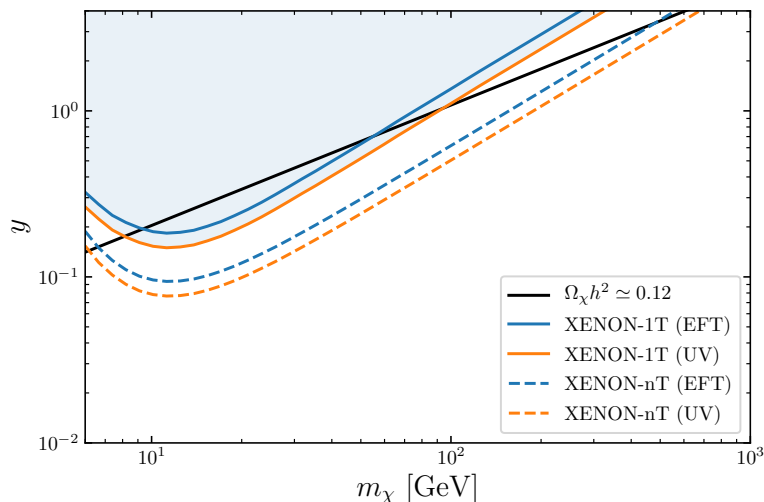


Figure 7. Constraints on the UV complete model defined in Eq. (3.7) for any charged lepton f and $m_\phi = 2m_\chi$. EFT/UV indicates that the curve takes the loop-induced dipole in Eq. (3.11)/(3.12).

similarly for the S case) indirect detection constraints are known to be weak as in this case the annihilation is of the p -wave type. But the bounds from dipole induced direct detection remains fully relevant, as given in Fig. 6 too.

Explicit UV complete models can be constrained according to the combination of effective operators they lead to. For the model considered in Sec. 3.2, which in a characteristic way gives both V and A interactions with similar weights, we show in Fig. 7 upper bounds on the Yukawa coupling y of Eq. (3.7), using the dipoles obtained in Eq. (3.11) (EFT) and Eq. (3.12) (UV). As previously discussed in Sec. 3.2, the difference between the two approaches shown in Fig. 7 is small. The current XENON-1T limit excludes the mass range $8.1 \text{ GeV} \lesssim m_\chi \lesssim 94 \text{ GeV}$ while future XENON-nT will be able to probe the $6.2 \text{ GeV} \lesssim m_\chi \lesssim 843 \text{ GeV}$ range.

As mentioned in the introduction, Ref. [16] also studied the direct detection signals that could be induced by four-fermion effective operators (involving two charged leptons) via DM-photon interactions induced at the one-loop level. This calculation was done by calculating the loop directly from the EFT and applying an $\overline{\text{MS}}$ prescription. Before concluding let us add a few comments on the several improvements we made here. Beside the fact that, strictly speaking, the divergences obtained at the pure EFT level cannot be removed applying this prescription (since there is no counterterm that could cancel the divergences, i.e. the result must be finite), opening the four-fermion blob as we did above shows that the results can largely depend on the way these effective interactions are generated (as shown by the s -channel example which gives vanishing results). The two-step calculation we did, calculating first the various moments that are induced and subsequently computing what it gives for direct detection (instead of calculating directly the direct detection cross section) is useful as it identifies for each case what kind of electromagnetic interactions is induced (with what it implies for each of these interactions). Phenomeno-

logically Fig. 4 also shows that the dramatic improvements of direct detection experiments in the last decade imply that the cases with chirality-flip suppressions (i.e. the S , P and T cases) are also testable (see e.g. the scalar case for $f = \tau$ in Fig. 4). As also shown above, electromagnetic interactions induced at the one-loop level are relevant not only for charged leptons but also for the heavy quark case.¹⁰

5 Conclusion

In the presence of four-fermion effective interactions of dark matter (DM) with Standard Model (SM) fermions, electromagnetic dipoles of DM can easily be generated, due to the loop process illustrated in Fig. 1. This is the case in particular if the operators are generated through the exchange of a t -channel mediator. We study systematically for all possible effective interactions the loop-induced dipoles and find that, if they are not identically vanishing, the electromagnetic dipoles in the WIMP paradigm are typically of the order of 10^{-21} (10^{-20}) ecm for vector (axial-vector) interactions, or of $10^{-20}m_f/m_\chi$ ecm for scalar, pseudo-scalar, and tensor interactions, see Eqs. (3.13)-(3.16). Calculations for a UV complete model give very similar results.

Via photon exchange such values imply observable nuclear recoil signals in direct detection experiments. This provides (or will provide) the most stringent constraints for various operators, in particular for axial or scalar operators, as well as for operators involving for instance muons. So far XENON-1T has excluded the loop-induced electromagnetic dipoles for some types of effective interactions in certain mass ranges—see Fig. 4. Future multi-ton liquid xenon experiments with substantially improved sensitivity will be able to probe the dipoles for all types of effective interactions over much broader mass ranges.

Acknowledgments

We thank Xiaoyong Chu and Laurent Vanderheyden for useful discussions. This work is supported by the “Probing dark matter with neutrinos” ULB-ARC convention and by the F.R.S./FNRS under the Excellence of Science (EoS) project No. 30820817 - be.h “The H boson gateway to physics beyond the Standard Model”.

A Loop calculations

In this appendix, we present the details of our loop calculations. Starting from Eq. (3.1), we first compute the traces:

$$\text{tr} \left[\frac{1}{\not{k}_2 - m_f} \gamma^\mu \frac{1}{\not{k}_1 - m_f} P_L \right] = 2m_f(k_1^\mu + k_2^\mu) D_k, \quad (\text{A.1})$$

$$\text{tr} \left[\frac{1}{\not{k}_2 - m_f} \gamma^\mu \frac{1}{\not{k}_1 - m_f} \gamma^\nu P_L \right] = 2 \left[k_1^\mu k_2^\nu + k_2^\mu k_1^\nu + (m_f^2 - k_2 \cdot k_1) g^{\mu\nu} - i \epsilon^{\mu\nu\rho\lambda} k_{1\rho} k_{2\lambda} \right] D_k, \quad (\text{A.2})$$

¹⁰For this case, it would be interesting to compute the loop-level direct detection signals that are induced via gluon exchange rather than photon exchange, which is beyond the scope of this work.

$$\text{tr} \left[\frac{1}{\not{k}_2 - m_f} \gamma^\mu \frac{1}{\not{k}_1 - m_f} \sigma^{\rho\lambda} P_L \right] = 2im_f \left[(k_1^\rho - k_2^\rho) g^{\lambda\mu} - \lambda \leftrightarrow \rho \right] + 2m_f \epsilon^{\lambda\mu\rho\nu} (k_1 - k_2)_\nu D_k, \quad (\text{A.3})$$

where

$$D_k \equiv \frac{1}{k_2^2 - m_f^2} \frac{1}{k_1^2 - m_f^2}. \quad (\text{A.4})$$

If P_L in the above traces is replaced by P_R , the results are similar except that $\epsilon^{\mu\nu\rho\lambda}$ and $\epsilon^{\lambda\mu\rho\nu}$ flip their signs.

Next, we plug the traces into the loop integral and integrate out k , assuming the mass hierarchy:

$$m_{\text{med}} \gg m_\chi \gg m_f. \quad (\text{A.5})$$

Taking the case of Eq. (A.1) with $G_X^{(t)}$ in Eq. (3.4) for example, we have:

$$\int \frac{d^4k}{(2\pi)^4} \text{tr} \left[\frac{1}{\not{k}_2 - m_f} \gamma^\mu \frac{1}{\not{k}_1 - m_f} P_L \right] \frac{1}{k^2 - m_{\text{med}}^2} \approx -\frac{iy^2}{16\pi^2} (p_1 + p_2)^\mu \frac{m_f}{m_{\text{med}}^2}. \quad (\text{A.6})$$

The loop integral is computed using `Package-X` [50] and expanded in q^2 , m_f , and m_χ . Only the leading order term is taken. Note that the integral is free from UV divergences because for $k \rightarrow \infty$ the integral behaves like $\int k^{-5} d^4k$.

With the result in Eq. (A.6) and $y^2/m_{\text{med}}^2 = \epsilon_a^L G_F$, we see that \mathcal{F}^μ introduced in Eq. (3.1) for $a = S$ and P should be

$$\mathcal{F}^\mu = \Gamma^a e Q_f \frac{\epsilon_a^L G_F m_f}{16\pi^2} (p_1 + p_2)^\mu. \quad (\text{A.7})$$

Then for $\bar{u}_2 \mathcal{F}^\mu u_1$, it can be decomposed into the form factors in Eq. (3.2) using the following identities:

$$\bar{u}_2 (p_1 + p_2)^\mu u_1 = \bar{u}_2 [i\sigma^{\mu\nu} q_\nu] u_1 + 2m_\chi \bar{u}_2 \gamma^\mu u_1 \quad (\text{A.8})$$

$$\bar{u}_2 (p_1 + p_2)^\mu i\gamma^5 u_1 = \bar{u}_2 [-\sigma^{\mu\nu} \gamma^5 q_\nu] u_1, \quad (\text{A.9})$$

where $q \equiv p_1 - p_2$. Eq. (A.8) is the well-known Gordon identity (due to the definition of q , our convention differs from that in Ref. [51] by a minus sign of q). Eq. (A.9) is similar but with additional γ^5 . It can be derived as follows:

$$\begin{aligned} \bar{u}_2 [i\sigma^{\mu\nu} \gamma^5 q_\nu] u_1 &= -\frac{1}{2} \bar{u}_2 [\gamma^\mu, \gamma^\nu] \gamma^5 q_\nu u_1 \\ &= -\frac{1}{2} \bar{u}_2 \left[\gamma^\mu \not{p}_1 \gamma^5 - \gamma^\mu \not{p}_2 \gamma^5 - \not{p}_1 \gamma^\mu \gamma^5 + \not{p}_2 \gamma^\mu \gamma^5 \right] u_1 \\ &= \frac{1}{2} \bar{u}_2 \left[(2p_2^\mu - \not{p}_2 \gamma^\mu) \gamma^5 + (2p_1^\mu - \gamma^\mu \not{p}_1) \gamma^5 \right] u_1 \\ &= (p_1 + p_2)^\mu \bar{u}_2 \gamma^5 u_1, \end{aligned} \quad (\text{A.10})$$

where in the second row the first and last terms cancel out because $\not{p}_1 \gamma^5 u_1 = -m_\chi \gamma^5 u_1$ and $\bar{u}_2 \not{p}_2 = \bar{u}_2 m_\chi$, and in the third row the $\not{p}_2 \gamma^\mu$ and $\gamma^\mu \not{p}_1$ terms cancel out for the same reason.

According to Eqs. (A.8) and (A.9), Eq. (A.7) generates magnetic and electric dipoles for $a = S$ and P , respectively. The values are already listed in Tab. 2. For other cases, the calculations are similar: We plug Eq. (A.2) or (A.3) into the loop integral to obtain \mathcal{F}^μ and use Eq. (A.8) or (A.9) to extract the dipole form factors. In general, when the resulting \mathcal{F}^μ contains \not{p}_1 and \not{p}_2 , after applying the Dirac algebra and on-shell conditions ($\not{p}_1 u_1 = m_\chi u_1$ and $\overline{u}_2 \not{p}_2 = \overline{u}_2 m_\chi$), they can be converted to linear combinations of $(p_1 + p_2)^\mu$ and $(p_1 - p_2)^\mu$. Terms containing the latter cancel out or can be neglected due to the Ward identity. In Package-X [50], the dipole form factors can be extracted using dedicated projectors, and we have verified that this approach leads to the same results.

As for the UV complete example introduced in Sec. 3.2, there are two diagrams contributing to the magnetic dipole: one with the photon coupled to the charge fermion f and the other with photon coupled to the charged scalar ϕ^\pm . We refer to the former and the latter as diagrams (i) and (ii), respectively. Their amplitudes read

$$\begin{aligned} i\mathcal{M}_{(i)} &= i \int \frac{d^4 k}{(2\pi)^4} \overline{u}_2 P_R \frac{1}{\not{k}_2 - m_f} i e Q_f \gamma^\mu \frac{1}{\not{k}_1 - m_f} P_L u_1 \varepsilon_\mu \frac{y y^*}{k^2 - m_\phi^2}, \\ i\mathcal{M}_{(ii)} &= i \int \frac{d^4 k}{(2\pi)^4} \overline{u}_2 P_R \frac{1}{\not{k} - m_f} P_L u_1 \varepsilon_\mu i e Q_\phi (k_1 + k_2)^\mu \frac{1}{k_1^2 - m_\phi^2} \frac{1}{k_2^2 - m_\phi^2} y y^*, \end{aligned} \quad (\text{A.11})$$

where Q_ϕ is the electric charge of ϕ^\pm . After integrating out the loop momentum, we find

$$\begin{aligned} \mathcal{M}_{(i)} &= \frac{e|y|^2 Q_f}{32\pi^2} \overline{u}_2 \gamma^\mu u_1 \varepsilon_\mu \left[\frac{1}{2\epsilon} + \frac{1}{4} + \log\left(\frac{\mu}{m_\phi}\right) \right] \\ &+ \frac{e|y|^2 Q_f}{32\pi^2 m_\phi^2} \overline{u}_2 \gamma^\mu u_1 \varepsilon_\mu \left[\frac{1}{2} m_\chi^2 - \frac{1}{2} m_f^2 \right] \\ &+ \frac{e|y|^2 Q_f}{32\pi^2 m_\phi^2} \overline{u}_2 i \sigma^{\mu\nu} q_\nu u_1 \varepsilon_\mu \left[-\frac{1}{3} m_\chi \right] \\ &+ [\overline{u}_2 \gamma^\mu \gamma^5 u_1 \text{ terms}], \end{aligned} \quad (\text{A.12})$$

$$\begin{aligned} \mathcal{M}_{(ii)} &= \frac{e|y|^2 Q_\phi}{32\pi^2} \overline{u}_2 \gamma^\mu u_1 \varepsilon_\mu \left[\frac{1}{2\epsilon} + \frac{1}{4} + \log\left(\frac{\mu}{m_\phi}\right) \right] \\ &+ \frac{e|y|^2 Q_\phi}{32\pi^2 m_\phi^2} \overline{u}_2 \gamma^\mu u_1 \varepsilon_\mu \left[\frac{1}{2} m_\chi^2 - \frac{1}{2} m_f^2 \right] \\ &+ \frac{e|y|^2 Q_\phi}{32\pi^2 m_\phi^2} \overline{u}_2 i \sigma^{\mu\nu} q_\nu u_1 \varepsilon_\mu \left[+\frac{1}{6} m_\chi \right] \\ &+ [\overline{u}_2 \gamma^\mu \gamma^5 u_1 \text{ terms}]. \end{aligned} \quad (\text{A.13})$$

Here $\overline{u}_2 \gamma^\mu \gamma^5 u_1$ terms are not important because they cancel out in the final result, as we have verified explicitly in the calculation.

As is manifest, the UV divergences in the first rows of Eqs. (A.12) and (A.13) cancel out when $Q_\phi + Q_f = 0$, which is required by the charge conservation of Eq. (3.7). What also cancel out in the remaining terms are those proportional to $\overline{u}_2 \gamma^\mu u_1$, which is expected because χ is neutral.

After all the cancellations, only the magnetic dipole terms exist. Comparing the last row of Eq. (A.12) to Eq. (3.11), we see that $\mathcal{M}_{(i)}$ reproduces the dipole obtained in the EFT approach. When the full theory is taken into account, the additional contribution due to $\mathcal{M}_{(ii)}$ is roughly half the size of the previous one, assuming $m_f \ll m_\chi$. Taking $Q_\phi = -Q_f$ and summing the two diagrams together, we obtain the result in Eq. (3.12).

References

- [1] G. Jungman, M. Kamionkowski, and K. Griest, *Supersymmetric dark matter*, *Phys. Rept.* **267** (1996) 195–373, [[hep-ph/9506380](#)].
- [2] G. Bertone, D. Hooper, and J. Silk, *Particle dark matter: Evidence, candidates and constraints*, *Phys. Rept.* **405** (2005) 279–390, [[hep-ph/0404175](#)].
- [3] J. L. Feng, *Dark Matter Candidates from Particle Physics and Methods of Detection*, *Ann. Rev. Astron. Astrophys.* **48** (2010) 495–545, [[1003.0904](#)].
- [4] G. Arcadi, M. Dutra, P. Ghosh, M. Lindner, Y. Mambrini, M. Pierre, S. Profumo, and F. S. Queiroz, *The waning of the WIMP? A review of models, searches, and constraints*, *Eur. Phys. J. C* **78** (2018), no. 3 203, [[1703.07364](#)].
- [5] L. Roszkowski, E. M. Sessolo, and S. Trojanowski, *WIMP dark matter candidates and searches—current status and future prospects*, *Rept. Prog. Phys.* **81** (2018), no. 6 066201, [[1707.06277](#)].
- [6] M. Schumann, *Direct Detection of WIMP Dark Matter: Concepts and Status*, *J. Phys. G* **46** (2019), no. 10 103003, [[1903.03026](#)].
- [7] G. Busoni, A. De Simone, E. Morgante, and A. Riotto, *On the Validity of the Effective Field Theory for Dark Matter Searches at the LHC*, *Phys. Lett. B* **728** (2014) 412–421, [[1307.2253](#)].
- [8] G. Busoni, A. De Simone, J. Gramling, E. Morgante, and A. Riotto, *On the Validity of the Effective Field Theory for Dark Matter Searches at the LHC, Part II: Complete Analysis for the s-channel*, *JCAP* **06** (2014) 060, [[1402.1275](#)].
- [9] G. Busoni, A. De Simone, T. Jacques, E. Morgante, and A. Riotto, *On the Validity of the Effective Field Theory for Dark Matter Searches at the LHC Part III: Analysis for the t-channel*, *JCAP* **09** (2014) 022, [[1405.3101](#)].
- [10] **XENON Collaboration**, E. Aprile *et al.*, *Dark Matter Search Results from a One Ton-Year Exposure of XENON1T*, *Phys. Rev. Lett.* **121** (2018), no. 11 111302, [[1805.12562](#)].
- [11] **LUX Collaboration**, D. S. Akerib *et al.*, *Results from a search for dark matter in the complete LUX exposure*, *Phys. Rev. Lett.* **118** (2017), no. 2 021303, [[1608.07648](#)].
- [12] **PandaX-II Collaboration**, X. Cui *et al.*, *Dark Matter Results From 54-Ton-Day Exposure of PandaX-II Experiment*, *Phys. Rev. Lett.* **119** (2017), no. 18 181302, [[1708.06917](#)].
- [13] M. Pospelov and T. ter Veldhuis, *Direct and indirect limits on the electromagnetic form-factors of WIMPs*, *Phys. Lett. B* **480** (2000) 181–186, [[hep-ph/0003010](#)].
- [14] K. Sigurdson, M. Doran, A. Kurylov, R. R. Caldwell, and M. Kamionkowski, *Dark-matter electric and magnetic dipole moments*, *Phys. Rev. D* **70** (2004) 083501, [[astro-ph/0406355](#)]. [Erratum: *Phys.Rev.D* 73, 089903 (2006)].

- [15] E. Masso, S. Mohanty, and S. Rao, *Dipolar Dark Matter*, *Phys. Rev. D* **80** (2009) 036009, [[0906.1979](#)].
- [16] J. Kopp, V. Niro, T. Schwetz, and J. Zupan, *DAMA/LIBRA and leptonically interacting Dark Matter*, *Phys. Rev. D* **80** (2009) 083502, [[0907.3159](#)].
- [17] T. Banks, J.-F. Fortin, and S. Thomas, *Direct Detection of Dark Matter Electromagnetic Dipole Moments*, [1007.5515](#).
- [18] A. L. Fitzpatrick and K. M. Zurek, *Dark Moments and the DAMA-CoGeNT Puzzle*, *Phys. Rev. D* **82** (2010) 075004, [[1007.5325](#)].
- [19] V. Barger, W.-Y. Keung, and D. Marfatia, *Electromagnetic properties of dark matter: Dipole moments and charge form factor*, *Phys. Lett. B* **696** (2011) 74–78, [[1007.4345](#)].
- [20] J.-F. Fortin and T. M. P. Tait, *Collider Constraints on Dipole-Interacting Dark Matter*, *Phys. Rev. D* **85** (2012) 063506, [[1103.3289](#)].
- [21] E. Del Nobile, C. Kouvaris, P. Panci, F. Sannino, and J. Virkajarvi, *Light Magnetic Dark Matter in Direct Detection Searches*, *JCAP* **08** (2012) 010, [[1203.6652](#)].
- [22] N. Weiner and I. Yavin, *How Dark Are Majorana WIMPs? Signals from MiDM and Rayleigh Dark Matter*, *Phys. Rev. D* **86** (2012) 075021, [[1206.2910](#)].
- [23] C. M. Ho and R. J. Scherrer, *Anapole Dark Matter*, *Phys. Lett. B* **722** (2013) 341–346, [[1211.0503](#)].
- [24] M. I. Gresham and K. M. Zurek, *Light Dark Matter Anomalies After LUX*, *Phys. Rev. D* **89** (2014), no. 1 016017, [[1311.2082](#)].
- [25] Y. Gao, C. M. Ho, and R. J. Scherrer, *Anapole Dark Matter at the LHC*, *Phys. Rev. D* **89** (2014), no. 4 045006, [[1311.5630](#)].
- [26] E. Del Nobile, G. Gelmini, P. Gondolo, and J.-H. Huh, *Generalized Halo Independent Comparison of Direct Dark Matter Detection Data*, *JCAP* **10** (2013) 048, [[1306.5273](#)].
- [27] E. Del Nobile, G. B. Gelmini, P. Gondolo, and J.-H. Huh, *Direct detection of Light Anapole and Magnetic Dipole DM*, *JCAP* **06** (2014) 002, [[1401.4508](#)].
- [28] J. Kopp, L. Michaels, and J. Smirnov, *Loopy Constraints on Leptophilic Dark Matter and Internal Bremsstrahlung*, *JCAP* **04** (2014) 022, [[1401.6457](#)].
- [29] X. Chu, J. Pradler, and L. Semmelrock, *Light dark states with electromagnetic form factors*, *Phys. Rev. D* **99** (2019), no. 1 015040, [[1811.04095](#)].
- [30] J. H. Chang, R. Essig, and A. Reinert, *Light(ly)-coupled Dark Matter in the keV Range: Freeze-In and Constraints*, *JHEP* **03** (2021) 141, [[1911.03389](#)].
- [31] X. Chu, J.-L. Kuo, and J. Pradler, *Dark sector-photon interactions in proton-beam experiments*, *Phys. Rev. D* **101** (2020), no. 7 075035, [[2001.06042](#)].
- [32] Y. Ali-Haïmoud, *Testing dark matter interactions with CMB spectral distortions*, *Phys. Rev. D* **103** (2021), no. 4 043541, [[2101.04070](#)].
- [33] M. Lindner, W. Rodejohann, and X.-J. Xu, *Coherent Neutrino-Nucleus Scattering and new Neutrino Interactions*, *JHEP* **03** (2017) 097, [[1612.04150](#)].
- [34] W. Rodejohann, X.-J. Xu, and C. E. Yaguna, *Distinguishing between Dirac and Majorana neutrinos in the presence of general interactions*, *JHEP* **05** (2017) 024, [[1702.05721](#)].

- [35] J. Goodman, M. Ibe, A. Rajaraman, W. Shepherd, T. M. P. Tait, and H.-B. Yu, *Constraints on Dark Matter from Colliders*, *Phys. Rev. D* **82** (2010) 116010, [[1008.1783](#)].
- [36] M. Bauer and T. Plehn, *Yet Another Introduction to Dark Matter: The Particle Physics Approach*, vol. 959 of *Lecture Notes in Physics*. Springer, 2019.
- [37] E. W. Kolb and M. S. Turner, *The Early Universe*, Addison-Wesley Publishing Company, 1990, USA.
- [38] P. Gondolo and G. Gelmini, *Cosmic abundances of stable particles: Improved analysis*, *Nucl. Phys. B* **360** (1991) 145–179.
- [39] **Particle Data Group Collaboration**, P. A. Zyla *et al.*, *Review of Particle Physics*, *PTEP* **2020** (2020), no. 8 083C01.
- [40] M. Nowakowski, E. A. Paschos, and J. M. Rodriguez, *All electromagnetic form-factors*, *Eur. J. Phys.* **26** (2005) 545–560, [[physics/0402058](#)].
- [41] C. Giunti and A. Studenikin, *Neutrino electromagnetic interactions: a window to new physics*, *Rev. Mod. Phys.* **87** (2015) 531, [[1403.6344](#)].
- [42] X.-J. Xu, *Tensor and scalar interactions of neutrinos may lead to observable neutrino magnetic moments*, *Phys. Rev.* **D99** (2019), no. 7 075003, [[1901.00482](#)].
- [43] C. Giunti and C. W. Kim, *Fundamentals of Neutrino Physics and Astrophysics*. Oxford University Press, 2007.
- [44] T. Lin, *Dark matter models and direct detection*, *PoS* **333** (2019) 009, [[1904.07915](#)].
- [45] J. I. Read, *The Local Dark Matter Density*, *J. Phys. G* **41** (2014) 063101, [[1404.1938](#)].
- [46] **XENON Collaboration**, E. Aprile *et al.*, *Projected WIMP sensitivity of the XENONnT dark matter experiment*, *JCAP* **11** (2020) 031, [[2007.08796](#)].
- [47] T. Hambye, M. H. G. Tytgat, J. Vandecasteele, and L. Vanderheyden, *Dark matter direct detection is testing freeze-in*, *Phys. Rev.* **D98** (2018), no. 7 075017, [[1807.05022](#)].
- [48] **MAGIC, Fermi-LAT Collaboration**, M. L. Ahnen *et al.*, *Limits to Dark Matter Annihilation Cross-Section from a Combined Analysis of MAGIC and Fermi-LAT Observations of Dwarf Satellite Galaxies*, *JCAP* **02** (2016) 039, [[1601.06590](#)].
- [49] **H.E.S.S. Collaboration**, H. Abdallah *et al.*, *Search for dark matter annihilations towards the inner Galactic halo from 10 years of observations with H.E.S.S.*, *Phys. Rev. Lett.* **117** (2016), no. 11 111301, [[1607.08142](#)].
- [50] H. H. Patel, *Package-X: A Mathematica package for the analytic calculation of one-loop integrals*, *Comput. Phys. Commun.* **197** (2015) 276–290, [[1503.01469](#)].
- [51] M. Peskin and D. Schroeder, *An Introduction to quantum field theory*, page 186, Addison-Wesley, 1995, USA.